CORA Cork Open Research Archive
Cartlann Taighde Oscailte Chorcaí

Title	Electronic impairment mitigation in optically multiplexed multicarrier systems
Authors	Zhao, Jian;Ellis, Andrew D.
Publication date	2011-02-01
Original Citation	ZHAO, J. & ELLIS, A. D. 2011. Electronic Impairment Mitigation in Optically Multiplexed Multicarrier Systems. Journal of Lightwave Technology, 29 (3), 278-290. doi: 10.1109/JLT.2010.2100806
Type of publication	Article (peer-reviewed)
Link to publisher's version	http://www.opticsinfobase.org/jlt/abstract.cfm?URI=jlt-29-3-278 - 10.1109/JLT.2010.2100806
Rights	© 2011 IEEE, Personal use of this material is permitted. Permission from IEEE must be obtained for all other uses, in any current or future media, including reprinting/republishing this material for advertising or promotional purposes, creating new collective works, for resale or redistribution to servers or lists, or reuse of any copyrighted component of this work in other works
Download date	2026-11-04 14:16:57
Item downloaded from	https://hdl.handle.net/10468/410

UCC
University College Cork, Ireland
Coláiste na hOllscoile Corcaigh


ucc
Coláiste na hOllscoile Corcaigh, Éire
University College Cork, Ireland

CORA
Cork Open Research Archive
Cartlann Taighde Oscailte Chorcaí

ZHAO, J. & ELLIS, A. D. 2011. Electronic Impairment Mitigation in Optically Multiplexed Multicarrier Systems. *Journal of Lightwave Technology*, 29 (3), 278-290.
doi: 10.1109/JLT.2010.2100806

© 2011 IEEE. Personal use of this material is permitted. Permission from IEEE must be obtained for all other uses, in any current or future media, including reprinting/republishing this material for advertising or promotional purposes, creating new collective works, for resale or redistribution to servers or lists, or reuse of any copyrighted component of this work in other works.

CORA Cork Open Research Archive http://cora.ucc.ie

Electronic Impairment Mitigation in Optically Multiplexed Multi-Carrier Systems

Jian Zhao and Andrew Ellis

Abstract— **In order to improve the performance of optically multiplexed multi-carrier systems with channel spacing equal to the symbol rate per carrier, we propose and systematically investigate an electronic signal processing technique to achieve near inter-channel crosstalk free and intersymbol-interference (ISI) free operation. We theoretically show that achieving perfect orthogonality between channels in these systems, together with ISI free operation as needed in generic communication systems, requires the shaping of the spectral profiles of not only the demultiplexing filter, but also the signal of each channel before demultiplexing. We develop a novel semi-analytical method to quantitatively analyze the levels of residual crosstalk and ISI arising from non-ideal system response in these systems. We show that by pre-filtering the signal to ensure that the system impulse response before channel demultiplexing approaches the targeted condition, the residual crosstalk due to imperfect orthogonality can be significantly mitigated and the necessity for carrier phase control in single-quadrature format based system can be relaxed. Further combining pre-filtering and receiver-side post-filtering to adaptively trim the demultiplexing filter enhances the performance. The use of the combined digital signal processing (DSP) in coherent-detection quadrature phase shifted keying (QPSK) based optically multiplexed multi-carrier system shows that this method outperforms conventional QPSK-based multi-carrier system without DSP or with only receiver-side DSP, especially when the responses of the transmitter and the demultiplexing filter are not precisely designed and the sampling rate of the analogue-to-digital converter is not sufficiently high. In addition, the inclusion of ISI free operation, with this aspect similar to the re-shaping method in conventional wavelength division multiplexing systems, allows the relaxation of the modulation bandwidth and chromatic dispersion compensation.**

Index Terms— **Modulation, orthogonal frequency division multiplexing, wavelength division multiplexing, detection**

I. Introduction

The rapid growth in video based Internet applications is increasing the demand for spectrally-efficient optical transmission systems. Spectral efficiency can be increased by either using higher-level modulation formats or reducing the channel spacing. According to information theory, it is possible to reduce the channel spacing to the symbol rate per carrier to achieve the Nyquist rate without any penalty from inter-channel crosstalk. In practice, this concept can be implemented in different scenarios, including either optically multiplexed optical orthogonal frequency division multiplexing (OFDM) [1], all-optical OFDM [2], no-guard-interval coherent optical OFDM [3-5], orthogonal wavelength division multiplexing (WDM) (OWDM) [6], and coherent WDM (CoWDM) [7-9], or electrically generated coherent optical OFDM (CO-OFDM) [10-11] and direct-detection based OFDM [12].

However, in all of these systems, due to the closely spaced channels, it is essential to ensure the orthogonality between channels such that they can be demultiplexed at the receiver without inter-channel crosstalk. Here, orthogonality is a broad concept as described in [13], and is not specific to the use of rectangular waveform. In electrically generated OFDM, discrete Fourier transform (DFT) based implementation [14] is usually employed. This DFT-based system uses a rectangular waveform with infinite spectral side lobes, which is one of solutions that satisfy the orthogonality. Although in practice, the infinite spectral tails are inevitably truncated by the bandwidth of modulators and receivers, the use of smaller symbol rate per carrier (~100Msym/s) in DFT-based OFDM with respect to the wider device bandwidth (~10-40GHz) ensures good approximation of the rectangular pulse shape and channel orthogonality. However, the complexity of DFT and the required operating speed of the optical modulator and receiver scale with the total symbol rate of the multiplexed OFDM signal, which limits the applications of this technique for ultra-wideband optical communications. In contrast, optically multiplexed systems multiplex and demultiplex channels using parallel optical modulators and receivers in the optical domain, such that the operating speed of the transmitters and receivers scales with the capacity of a single channel rather than the total capacity. Consequently, the speed bottleneck at the electronic interfaces is eliminated. This implementation is similar to the filter-bank based OFDM in wireless communications [13]. However, due to a high symbol rate per carrier (~10-40Gsym/s) in these systems, a rectangular pulse with infinite spectral tails cannot be achieved by practical device, which commonly has a bandwidth less than 50GHz. Therefore, other bandwidth limited solutions excluding the rectangular pulse have to be used, which, however, are still difficult to be achieved by using a combination of analogue optical and electrical devices. Consequently, given the limitations of current manufacturing

Manuscript received June 30, 2010. This work was supported by Science Foundation Ireland under grant number 06/IN/I969.

Jian Zhao and Andrew Ellis are with Photonic Systems Group, Tyndall National Institute, University College Cork, Lee Maltings, Prospect Row, Cork, Ireland (e-mail: jian.zhao@tyndall.ie).

Digital Object Identifier: xxxx

technologies, residual inter-channel crosstalk exists even with careful optimization of for example the optical filter bandwidth. To enable optically multiplexed multi-carrier systems, several techniques were proposed. For single-quadrature modulation formats, the penalties arising from the residual crosstalk may be reduced by extra control of the phase difference between channels. This technique is known as CoWDM [7-9]. However, as reported in previous experiments [2-4] and will be theoretically shown in this paper, such phase control cannot be used to mitigate the penalties in two-quadrature formats, such as no-guard-interval coherent optical OFDM [3-4]. Consequently, several other methods were proposed to mitigate the impact of inter-channel crosstalk, including smaller number of carriers (e.g. two-channel quadrature phase shifted keying (QPSK) based OFDM [2-3]), optical filtering strategy to approximate DFT [15], or the use of a digital signal processing (DSP) based filter with sufficiently high sampling rate (4samples/sym) at the receiver [4-5]. Note that although the term "OFDM" is used in some of these optically multiplexed systems, different from DFT-based OFDM, these systems do not realize "ideal" orthogonality that is required for OFDM so residual crosstalk exists. Therefore, in this paper, we will avoid the use of the term "OFDM" except when citing prior work in the literature.

Despite various experimental demonstrations in optically multiplexed multi-carrier systems with channel spacing equal to the symbol rate per carrier, most systems aim to optimize the receiver-side optical/electrical filter to mitigate the impairments. However, different from the matched filter theory [16-17] which does not place restrictions on the transmitted signal pulse shape, or Nyquist ISI criterion [17] where the freedom to select the transmitted signal pulse shape is large, achieving perfect channel orthogonality in these systems, together with ISI free operation, requires the shaping of the spectral profiles of not only the demultiplexing filter, but also the signal of each channel before demultiplexing. Note that re-shaping has been widely used in optical communications for CD compensation [18], ISI mitigation in conventional bandwidth-limited WDM [19], and Nyquist WDM [20]. Among them, re-shaping in Nyquist WDM is the most similar to that investigated in this paper, considering not only ISI but also the channel orthogonality. However, this technique does not realize channel spacing equal to the symbol rate per carrier.

In this paper, we will extend our previous work [21] and provide a generalized framework for optically multiplexed multi-carrier systems with channel spacing equal to the symbol rate per carrier. We derive the orthogonality condition for these systems by using a different mathematical manipulation from that in [13], and propose a novel semi-analytical method that is able to quantitatively analyze the residual crosstalk and ISI levels arising from the non-ideal system response. From this analysis, the major similarities and unique features of different implementations reported recently are apparent. We then study the re-shaping method using two typical examples. We investigate the use of electronic pre-filtering in OOK-based system, and show that this method can greatly reduce the level of the inter-channel crosstalk. Consequently, the technique of CoWDM [7-9], with additional phase control to mitigate the impact of residual crosstalk in single-quadrature formats, is not required. QPSK-based system is chosen as the second example, and we numerically illustrate that further combining pre-filtering with receiver-side DSP enhances the approach to the targeted condition, and consequently outperforms conventional QPSK-based no-guard-interval coherent OFDM without DSP [2-3] and with only receiver-side DSP [4]. This performance improvement can be achieved even for a receiver sampling rate as low as 2samples/sym. In addition, the inclusion of ISI free operation, with this aspect similar to that in conventional WDM systems [18-19], allows the relaxation of the modulation bandwidth and CD compensation.

The paper is organised as follows: in Section II, we describe the principle of system design, including the extension of the known condition for ISI free operation to crosstalk free operation for multi-carrier systems with channel-spacing equal to the symbol rate per carrier, and a semi-analytical method to analyze the residual crosstalk and ISI levels. In Section III, pre-filtering is used to trim the system response before demultiplexing, and its performance is investigated in direct-detection OOK based system. This example illustrates that by fundamentally reducing the crosstalk level, CoWDM, with phase control to mitigate the impact of the crosstalk, is not required. The overall benefits of the DSP method are emphasized in Section IV, where the pre-filtering method used in Section III is combined with post-filtering to obtain near inter-channel crosstalk and ISI free operation in QPSK-based multi-carrier system. Finally, Section V summarizes the results.

II. Principle of System Design

In order to develop the electronic signal processing technique to improve the system performance, it is critical to identify the condition to enable crosstalk and ISI free operation and consequently obtain the guideline on the design of DSP to approach this condition. It would also be essential to develop a method that, in the existence of residual crosstalk and ISI due to non-ideal system response (applicable to the practical systems), can quantitatively analyze the levels of these impairments.

a. System Design for Crosstalk-Free Operation

The condition for ISI-free operation of a particular channel, also called Nyquist ISI criterion [17], is similar to that in the single-channel case, so in this sub-section, we will mainly focus on the derivation of the condition for inter-channel crosstalk free operation or channel orthogonality specific to the multi-carrier systems with channel spacing reduced to the symbol rate per carrier. We define $E_j(t)$ as the optical field of the signal after the demultiplexing filter targeted to demultiplex the j^{th} channel. Here, $E_j(t)$ is the baseband representation:

$$E_j(t) = E_0 \sum_{k=1}^{J} \sum_{n=-\infty}^{\infty} a_{k,n} I_{k,j}(t - nT) e^{i(\omega_k - \omega_j)\cdot nT + i\phi_k} \qquad (1)$$

where E_0 and J are an optical field constant and the number of channels respectively. $a_{k,n}$ is the n^{th} logic data for the k^{th} channel. T, ω_k, and ϕ_k are the symbol period, the frequency and phase of the k^{th} carrier respectively. $I_{k,j}(t)$ is the signal pulse of the k^{th} channel after the filter targeted to demultiplex the j^{th} channel, and represents the overall impulse response of the whole system. $I_{k,j}(t)$ is related to the baseband spectral profile of the signal before demultiplexing, $H_s(\omega)$, and the transfer function of the demultiplexing filter for the j^{th} channel, $H_{D,j}(\omega+\omega_j)$, by:

$$I_{k,j}(t)=\frac{1}{2\pi}\int_{-\infty}^{+\infty}H_s(\omega-\omega_k+\omega_j)H_{D,j}(\omega+\omega_j)e^{i\omega t}d\omega$$

$$\text{or}\qquad H_{overall,k,j}(\omega)=H_s(\omega-\omega_k+\omega_j)\cdot H_{D,j}(\omega+\omega_j) \tag{2}$$

where $H_{\text{overall},k,j}(\omega)$ is the Fourier transform of $I_{k,j}(t)$. $H_s(\omega)$ here represents the overall system response before demultiplexing, including the transmitted electrical signal pulse shape, the transfer functions of the driving amplifier and the modulator, CD in the fiber link etc. The proposed pre-shaping technique, by employing a simple finite impulse response (FIR) filter at the transmitter, ensures that $H_s(\omega)$ approaches the desirable profile as will be described later. $H_{D,j}(\omega+\omega_j)$ here represents the receiver-side optical filter for channel demultiplexing, but, in coherent detection, should include both the optical filtering, $H_{opt,j}(\omega+\omega_j)$, and the electrical filtering, $H_{ele,j}(\omega+\omega_j-\omega_{lo})$:

$$H_{D,j}(\omega+\omega_j)=H_{opt,j}(\omega+\omega_j)\cdot H_{ele,j}(\omega+\omega_j-\omega_{lo}) \tag{3}$$

where ω_{lo} is the frequency of the local oscillator. Consequently, receiver-side DSP can be used to precisely trim $H_{D,j}(\omega+\omega_j)$ to the targeted spectral profile. The targeted spectral profiles for $H_s(\omega)$ and $H_{D,j}(\omega+\omega_j)$ will be those satisfying the conditions for both ISI and crosstalk free operation, as will be shown in (6) and (9). Note that in practice, $H_{D,j}(\omega+\omega_j)$ is also usually matched to $H_s(\omega)$, i.e. $H_{D,j}(\omega+\omega_j)=H_s^*(\omega)$, to minimize the noise impact. In this case, the freedom is further reduced and the problem is degenerated to the design of only $H_s(\omega)$ to satisfy (6) and (9).

It is evident that in the systems under investigation, due to the closely spaced channels, the demultiplexing filter for the channel j, $H_{D,j}(\omega+\omega_j)$, may pass through the signals of the adjacent channels, e.g. channel j-1 and j+1, in addition to the targeted channel, such that $I_{k,j}(t)$ ($k\neq j$) is not zero for all t. However, the symbol decisions are made only based on the final samples of the signal, where the final decision samples are those obtained after all over- or non-over-sampling based digital processing in coherent detection, or the baseband field at the sampling point in direct detection. Consequently, we only require that the crosstalk and ISI levels at the final sampling points, mT, are zero. By setting $t=mT$ in (1), we have:

$$E_j(mT)=E_0a_{j,m}I_{j,j}(0)e^{i\phi_j}+E_0\sum_{n\neq m}a_{j,n}I_{j,j}((m-n)T)e^{i\phi_j}+E_0\sum_{k\neq j}\sum_{n}a_{k,n}I_{k,j}((m-n)T)e^{i\phi_k} \tag{4}$$

Here we use the property that the channel spacing satisfies $(\omega_k-\omega_j)=2\pi p/T$, where p is an integer. The first, second, and third terms on the right-hand of (4) represent the signal level, ISI, and the crosstalk. Define the folded spectrum of $I_{k,j}(t)$, $FH_{\text{overall},k,j}(\omega)$:

$$FH_{\text{overall},k,j}(\omega)=\sum_{p=-\infty}^{+\infty}H_{overall,k,j}(\omega+\frac{2\pi p}{T}) \tag{5}$$

The condition for ISI free operation for the channel j is similar to that in single-channel or conventional WDM systems and requires that the folded spectrum of $I_{j,j}(t)$ satisfies [17]:

$$FH_{overall,j,j}(\omega)=const.\qquad \text{for } \omega\in[-\pi/T\ \pi/T] \tag{6}$$

where the *const.* is not zero. Intuitively, (6) can be understood that the frequency shifted replicas of $H_{\text{overall},j,j}(\omega)$ must add up to a constant value. This implies that only particular set of signal pulse shapes with associated matched receiver filters can enable ISI free operation. Fortunately, the selection of signal pulse shape under this restriction is not stringent, and many pulse shapes satisfy (6) such that the signal generated from practical transmitters in conventional WDM can obtain ISI free operation without pre-filtering, unless the system is bandwidth limited [19], or the signal is distorted by CD [18]. Fig. 1 illustrates an example using a sinc function for both $H_s(\omega)$ and $H_{D,j}(\omega+\omega_j)$. This pair of functions satisfies (6), therefore achieving ISI free operation, as depicted by the middle row in the figure. Note that in this example, $H_{D,j}(\omega+\omega_j)$ is also a matched filter of $H_s(\omega)$, resulting in not only ISI free but also minimized noise.

On the other hand, in order to enable crosstalk-free operation, the last term in (4) should be zero for any possible value of $a_{k,n}$

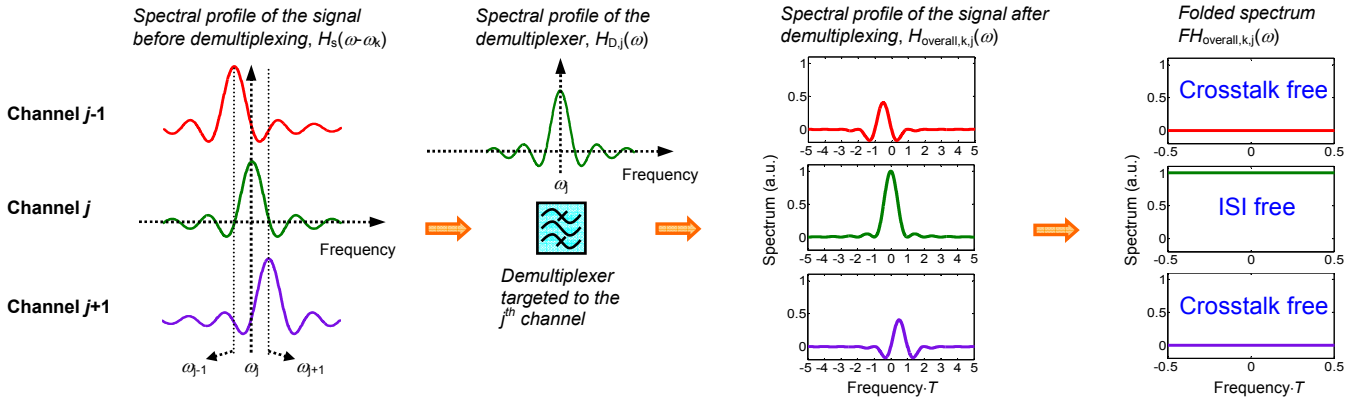


Fig. 1: An example to illustrate the condition for crosstalk and ISI free operation using a pair of sinc functions. The first, third, and fourth columns show the spectral profiles of the signals before demultiplexing, after demultiplexing, and after the spectra folding respectively, when the input signal is the $(j\text{-}1)^{th}$ (top), j^{th} (middle), and $(j\text{+}1)^{th}$ (bottom) channels. The second column shows the spectral profile of the demultiplexing filter targeted to the j^{th} channel.

and any channel $k \neq j$, which is equivalent to:

$$I_{k,j}(lT)=0 \text{ for any integer } l \text{ and any } k \neq j \tag{7}$$

Taking the Fourier transform of $I_{k,j}(lT)$, we obtain:

$$\begin{aligned} I_{k,j}(lT) &= \frac{1}{2\pi}\int_{-\infty}^{+\infty} H_{overall,k,j}(\omega)e^{i\omega lT}d\omega \\ &= \frac{1}{2\pi}\int_{-\pi/T}^{\pi/T}\sum_{p=-\infty}^{+\infty} H_{overall,k,j}(\omega+\frac{2\pi p}{T})e^{i\omega lT}d\omega \end{aligned} \tag{8}$$

Equation (8) implies that $I_{k,j}(lT)$ is proportional to the Fourier series coefficients of $FH_{overall,k,j}(\omega)$. From (7) and (8), it can be derived that to enable crosstalk-free operation, we require:

$$\begin{aligned} FH_{overall,k,j}(\omega) = T\{&I_{k,j}(0)+I_{k,j}(-T)e^{i\omega T}+I_{k,j}(T)e^{-i\omega T} \\ &+I_{k,j}(-2T)e^{2i\omega T}+I_{k,j}(2T)e^{-2i\omega T}+\ldots\}=0 \end{aligned} \tag{9}$$

where $\omega \in [-\pi/T\ \pi/T]$ and $k \neq j$

The requirements to satisfy not only (6) (Nyquist ISI criterion) but also (9) (channel orthogonality) result in largely reduced freedom to select the signal pulse shape and the associated demultiplexing filter. A pair of sinc functions illustrated in Fig. 1 satisfies not only (6) but also the condition (9) for channel orthogonality, as depicted by the demultiplexed and folded spectra for channel j-1 (top row) and j+1 (bottom row). This pair of functions is used for DFT-based electrical OFDM. However, it might not be suitable for optically multiplexed systems because the rise time (or finite bandwidth) of the analogue devices, e.g. amplifiers, modulators, and receivers etc, prevents the achievement of these functions. Fig. 2 shows another two pairs of spectral profiles that satisfy both (6) and (9). In a more general form, the restriction placed by (6) and (9) for this set of solutions is that $H_s(\omega)\times H_{D,j}(\omega+\omega_j)$ is a rectangular shape with bandwidth of $1/T$, i.e. any pair of $H_s(\omega)$ and $H_{D,j}(\omega+\omega_j)$ under this restriction achieves ISI and crosstalk free operation. However, to also minimize the noise impact, $H_{D,j}(\omega+\omega_j)$ is desirable to be a matched filter of $H_s(\omega)$ [16], so in practice, $H_s(\omega)$ and $H_{D,j}(\omega+\omega_j)$ should be both as rectangular as possible. A pair of rectangular functions has been used in Nyquist WDM [20]. However, this technique uses optical filters to approach the rectangular spectral profiles. Precluded by the limitations of the device fabrication, it does not achieve channel spacing equal to the symbol rate per carrier. In Section III and IV, we will employ simple FIR filters to approach the rectangular function with infinite slopes and achieve near crosstalk and ISI free operation in optically multiplexed multi-carrier systems.

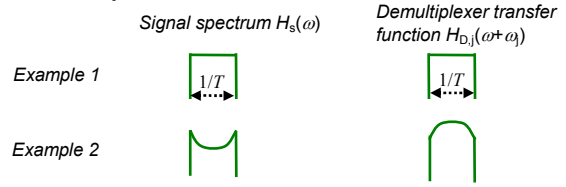


Fig. 2. Another two examples that achieve crosstalk and ISI free operation.

It is noted that guard interval (GI) is not included in the above derivations. GI is usually added to the multiplexed signal and subtracted before demultiplexing in DFT-based OFDM such as CO-OFDM [10] for CD compensation. However, it is not commonly used in optically multiplexed systems including all-optical OFDM [2], CoWDM [7-9] and no-guard-interval OFDM [3-5], because in these systems, it is difficult to add GI after channel multiplexing and CD is usually compensated using digital filters without overhead.

b. A Semi-Analytical Method to Analyze Residual Crosstalk

From (4), we can see that the crosstalk from the adjacent k^{th} ($k \neq j$) channel into a particular sample (the m^{th} sample) of the targeted j^{th} channel may contain the contributions from any symbol (n^{th}) of the adjacent channel, $a_{k,n}\cdot I_{k,j}((m-n)T)\cdot\exp(j\phi_k)$. On the other hand, from (9), we can see that if residual crosstalk exists due to imperfect system response, $T\cdot I_{k,j}((m-n)T)$ is equal to the $(n-m)^{th}$ Fourier series coefficient of $FH_{overall,k,j}(\omega)$. Therefore, we can develop the procedure to analyze the residual crosstalk as follows:

1. Obtain the spectral profiles of the channel signal before demultiplexing, $H_s(\omega)$, and the demultiplexing filter, $H_{D,j}(\omega+\omega_j)$, by calculations or simulations;
2. Calculate the folded spectrum $FH_{overall,k,j}(\omega)$, where k is j and any channel around the channel j that is within the scope of analysis;
3. Take Fourier transform to obtain the Fourier series coefficients, $F_{k,j}(n-m)$, of the folded spectrum;
4. The amount of crosstalk from the n^{th} symbol of the k^{th} channel into the m^{th} sample of the j^{th} channel is $a_{k,n}F_{k,j}(n-m)\cdot\exp(j\phi_k)/T$;
5. The signal level on the m^{th} sample and the amount of ISI from the n^{th} symbol to the m^{th} sample are $a_{j,m}F_{j,j}(0)\cdot\exp(j\phi_j)/T$ and $a_{j,n}F_{j,j}(n-m)\cdot\exp(j\phi_j)/T$ respectively.

We define two parameters, signal to crosstalk power ratio (SCPR) and signal to ISI power ratio (SIPR):

$$SCPR=\frac{|I_{j,j}(0)|^2}{\sum_{k\neq j}\sum_{p}|I_{k,j}(p)|^2} \quad \text{and} \quad SIPR=\frac{|I_{j,j}(0)|^2}{\sum_{p\neq 0}|I_{j,j}(p)|^2} \tag{10}$$

These definitions avoid the parameter dependence on the data pattern $a_{k,n}$, so can be used in any modulation format to quantitatively evaluate the total amount of impairments.

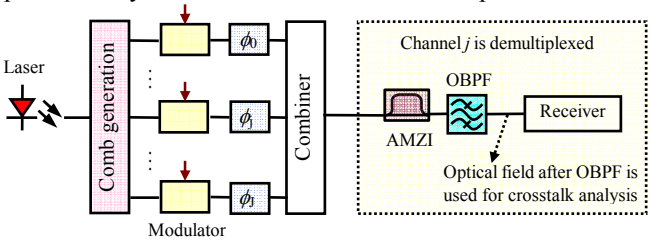


Fig. 3. An example system for crosstalk analysis.

To illustrate the procedure described above, as an example, we calculate the crosstalk and ISI levels by employing a typical setup used in conventional CoWDM and no-guard-interval OFDM [2-3, 7-9], as shown in Fig. 3. Optical carriers with 10GHz spacing are modulated by Mach-Zehnder modulators (MZMs) using 10Gsym/s raised-cosine shaped electrical signals with a roll-off coefficient of 0.4. The equivalent transfer

function of the driving amplifier and the MZM electronic interface is 10GHz 5th-order Bessel shaped. The demultiplexing filter for channel j consists of an asymmetric Mach-Zehnder interferometer (AMZI) with a free spectral range (FSR) of 20GHz and a 3rd-order Gaussian-shaped optical band-pass filter (OBPF). The bandwidth of the OBPF is varied for investigation. Modulation format is not specified in this example, so the calculated results, as will be shown in Fig. 4&5 and Table 1, are applied to any format. In addition, the detection method is not specified and the crosstalk analysis is based on the optical field of each channel after OBPF. Therefore, the results are applied to both direct and coherent detections. Note however that the impact of the obtained crosstalk level on the required optical signal-to-noise ratio (OSNR) would be a function of both the modulation format and the detection method. Finally, it is noted that in coherent detection with post processing, the analysis can also include the effects of receiver-side DSP (see (3)).

Figure 4 shows the folded spectra, $FH_{\text{overall,k,j}}(\omega)$, of the targeted channel j ((b)) and its two adjacent channels j-1 ((a)) and j+1 ((c)) when the OBPF bandwidth is 20GHz. Unlike the folded spectra in Fig. 1, $FH_{\text{overall,k,j}}(\omega)$ in Fig. 4 is not perfectly constant for the j^{th} channel, and zero for the adjacent channels, resulting in residual crosstalk and ISI.

The crosstalk and ISI coefficients normalized to that of the signal for the m^{th} sample of the j^{th} channel, mathematically represented as $I_{\text{k,j}}((m\text{-}n)T)/I_{\text{j,j}}(0)$, are calculated according to the procedure and Fig. 4, and are shown in Table 1. In the table, the crosstalk and ISI coefficients for *i*) the symbols with one or more symbols apart from the m^{th} sample, and *ii*) the channels with two or more channels apart from the j^{th} channel, are less than 0.002, so are neglected.

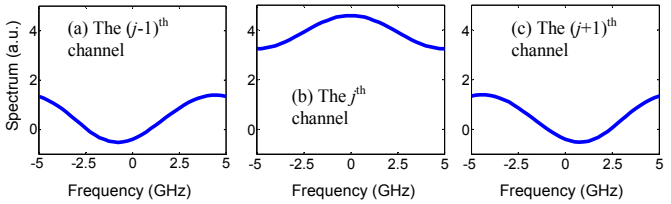


Fig. 4. The folded spectra, $FH_{\text{overall,k,j}}(\omega)$, for (b) the targeted channel j, and its two adjacent channels (a) (j-1) and (c) (j+1) in the system as described above.

Table 1. The normalized crosstalk and ISI coefficients for the m^{th} sample of the j^{th} channel, $I_{\text{k,j}}((m\text{-}n)T)/I_{\text{j,j}}(0)$. The OBPF bandwidth is 20GHz.

	the contribution of the $(m\text{-}1)^{\text{th}}$ bit	the contribution of the m^{th} bit	the contribution of the $(m\text{+}1)^{\text{th}}$ bit
channel j-2	0.024+0.003j	-0.024	0.024-0.003j
channel j-1	-0.113-0.05j	0.124	-0.113+0.05j
channel j	0.087	1	0.087
channel j+1	-0.113+0.05j	0.124	-0.113-0.05j
channel j+2	0.024-0.003j	-0.024	0.024+0.003j

The SCPR and SIPR are also calculated accordingly, as shown in Fig. 5, which depicts SCPR and SIPR versus the OBPF bandwidth. As expected, SIPR increases with the OBPF bandwidth, and is larger than 18dB provided that a bandwidth with more than 20GHz is used. In contrast, SCPR is below 15dB even for a bandwidth as small as 5GHz. The SCPR gradually decreases to 10dB as the OBPF bandwidth increases to around 18GHz, after which the SCPR is improved somewhat. This improvement is due to the fact that an OBPF with a wider bandwidth beyond 18GHz would pass through not only the main spectral lobe of the adjacent channels j-1 and j+1 with positive spectral amplitude, but also the side lobes with negative spectral value, such that the overall crosstalk level from the adjacent channels j-1 and j+1 is reduced. When the OBPF bandwidth is further increased beyond 25GHz, the crosstalk from the channels j-2 and j+2 becomes dominant, resulting in severely degraded SCPR.

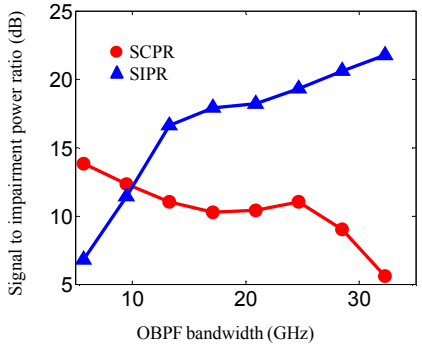


Fig. 5. SCPR and SIPR as a function of the OBPF bandwidth for the system as described above.

SCPR and SIPR cannot fully represent the influence of the impairments on system performance. In earlier work, the impact of crosstalk with random channel phase in conventional WDM was numerically investigated [22]. In multi-carrier systems with channel spacing equal to the symbol rate per carrier, it has been experimentally observed that the penalties arising from the residual crosstalk depend on the phase difference between optical carriers in single-quadrature formats such that extra phase control can improve the performance [7-9]. In contrast, this improvement by phase control was not observed in QSPK-based multi-carrier systems such as all-optical OFDM [2] and no-guard-interval coherent optical OFDM [3-4]. These phenomena can be understood from (4). For simple illustration, we employ the data in Table 1, and re-write (4) while only considering the crosstalk terms from the channels j-1 and j+1:

$$\begin{aligned} E_j(mT) \propto\ & (a_{j,m} + 0.087\cdot a_{j,m-1} + 0.087\cdot a_{j,m+1})e^{i\phi_j} \\ & + (0.124\cdot a_{j-1,m} + (-0.113-0.05j)\cdot a_{j-1,m-1} + (-0.113+0.05j)\cdot a_{j-1,m+1})e^{i\phi_{j-1}} \\ & + (0.124\cdot a_{j+1,m} + (-0.113+0.05j)\cdot a_{j+1,m-1} + (-0.113-0.05j)\cdot a_{j+1,m+1})e^{i\phi_{j+1}} \end{aligned} \quad (11)$$

From (11), we can see that real components dominate the coefficients of the crosstalk terms. Furthermore, in single-quadrature formats, the data values are real. Fig. 6(a)-(b) show the diagrams when the phase difference between channels (i.e. ϕ_{j-1}-ϕ_j and ϕ_{j+1}-ϕ_j) is (a) $\pi/2$ and (b) 0 in OOK-based system. The points in the figure are obtained by calculating (11) for all possible data values. It can be seen that setting the phase difference between channels to be $\pi/2$ causes that the signal and the crosstalk to be approximately orthogonal, and consequently improve the system performance. Note that this "orthogonal" is different from the channel "orthogonality" as described above and should not be mixed in the concept. This improvement by phase control is not applicable to the QPSK format, where $a_{\text{k,n}}$ is complex. Fig. 6(c) depicts the diagram for the QPSK signal.

This constellation is weakly dependent on the phase, so only the case for ϕ_{j-1}-ϕ_j (and ϕ_{j+1}-ϕ_j) of $\pi/2$ is plotted in the figure.

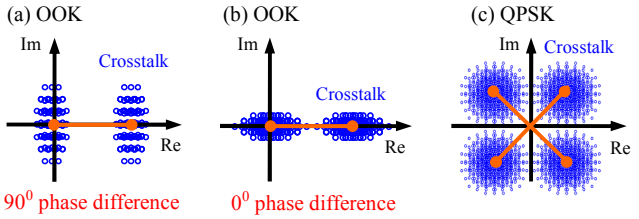


Fig. 6. Constellation diagrams for an OOK signal ((a) and (b)) with ϕ_{j-1}-ϕ_j (and ϕ_{j+1}-ϕ_j) of (a) $\pi/2$ and (b) 0, and a QPSK signal ((c)) with ϕ_{j-1}-ϕ_j (and ϕ_{j+1}-ϕ_j) of $\pi/2$. The points are obtained by calculating (11) for each data value.

The feature that the penalty can be mitigated by extra phase control in OOK format also results in a slightly narrower optimized OBPF bandwidth than that for the QPSK format. Simulations show that the optimal OBPF bandwidths for the conventional OOK and QPSK systems are around 20GHz and 25GHz respectively. From Fig. 5, it can be seen that a 25GHz OBPF bandwidth achieves a tradeoff between the crosstalk and ISI, with 11dB SCPR and 19dB SIPR. However, in OOK-based system with the optimized phase difference $\pi/2$, the performance is more sensitive to the crosstalk from the channels j-2 and j+2. Consequently, a narrower OBPF bandwidth is optimal to reduce the crosstalk from the channels j-2 and j+2, with no evident performance degradation arising from a higher crosstalk level from the channels j-1 and j+1 by phase control.

III. Pre-Shaping Technique For Crosstalk Mitigation

Based on the implications of previous analysis, in this section, we will study the pre-shaping method in OOK-based multi-carrier system with channel spacing equal to the symbol rate per carrier, and show that by fundamentally reducing the crosstalk level, conventional CoWDM [7-9], with phase control to mitigate the impact of residual crosstalk in single-quadrature formats, is not required. The proposed method also relaxes the modulation bandwidth and enhances the CD tolerance.

Figure 7 shows the simulation setup, which was implemented using Matlab. A continuous wave (CW) light from a distributed-feedback (DFB) laser with 100kHz linewidth was fed into an optical comb generator to obtain five carriers with equal intensities and phases. The channel spacing was 10GHz, equal to the symbol rate per carrier. The signal data trains consisted of 10Gbit/s 2^{11}-1 pseudo-random binary sequences (PRBS) repeated 5 times (10,235 bits) and different delays were applied to the five channels so that their bit sequences were uncorrelated. These logic data trains were up-sampled to two samples per symbol and pre-filtered by 2samples/sym FIR filter to create the desirable signal spectral profile according to the prior knowledge of the system response before channel demultiplexing. Because CD compensation was incorporated in the pre-filtering in this paper, the output signals could be complex. These pre-filtered signals were D/A converted with 8-bit physical resolution, unless otherwise stated. The 2samples/sym signals were further up-sampled, with each sample generating a 20-sample rectangular pulse (40 samples per symbol), to emulate the analogue signals. The DAC had 8GHz bandwidth and 2nd-order Gaussian-shaped spectral profile. The frequency response of the DACs was compensated during the pre-filtering. The analogue signal outputs of the DACs were amplified and used for data modulation. The input electrical signal level into the modulators was varied to investigate the nonlinear effect during modulation. The equivalent frequency response of the driving amplifier and the modulator's electronic interface was 5th-order Bessel shaped with 10GHz bandwidth, unless otherwise stated. The phases of the modulated optical signals were controlled to be $\phi_k=(k\text{-}1)\cdot\phi$, k=1…5 for investigation. Note that these phase controls were not needed in the pre-filtered system, as will shown in Fig. 8&9.

The transmission link comprised 80km single-mode fiber (SMF) spans, with fiber loss of 0.2dB/km, CD of 16ps/km/nm, and nonlinear coefficient of 1.2/W/km. The split-step Fourier method was used to calculate the signal propagation in the fibers. The step length was 1km at 0dBm signal launch power per channel, and was varied linearly with the input power. These step lengths were sufficient to ensure calculation accuracy. At the end of each span, amplified spontaneous emission (ASE) noise from optical amplifiers was modeled as complex additive white Gaussian noise with a spectral density of $n_{sp}h\nu(G\text{-}1)$ for each polarization, where G and $h\nu$ are the gain and the photon energy respectively. n_{sp} is the population inversion factor of the amplifiers and was set to give a 4dB noise figure (NF).

The noise of the optical preamplifier was also modeled as an additive white Gaussian noise for each polarization state. The launch power into the preamplifier was adjusted to control the OSNR. In this section, a single-stage 3rd-order Gaussian-shaped

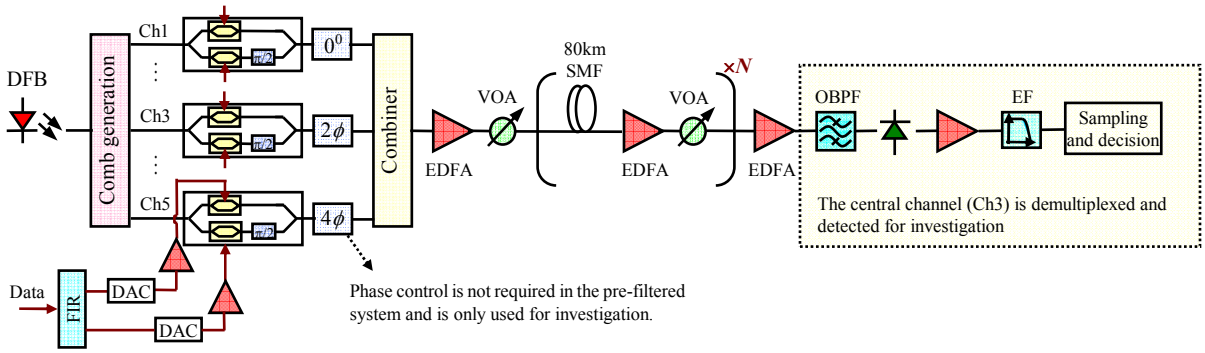


Fig. 7: Simulation setup of the pre-shaping technique in a five-channel OOK-based system with channel spacing equal to the symbol rate per carrier

OBPF with a 9GHz bandwidth was used for demultiplexing. The demultiplexed signal was directly detected. The power of the signal into the photodiode was -3dBm and the thermal noise spectral power density of the photodiode was 20pA/Hz$^{1/2}$. After detection, the signal was electrically amplified, filtered by a 15GHz 4th-order Bessel electrical filter (EF), and sampled for data decision using optimal threshold decoding.

For comparison, conventional OOK-based CoWDM [7] was also implemented. Channel multiplexing and demultiplexing were depicted in Fig. 3 while the transmission link was the same as that in Fig. 7. The electrical data trains were raised-cosine shaped with a roll-off coefficient of 0.4. These signals were fed directly into the driving amplifiers and modulated by MZMs. The phases of the modulated optical signals were controlled to be $\phi_k=(k\text{-}1)\cdot\phi$, k=1…5. The demultiplexing filter comprised an AMZI with 20GHz FSR to separate the even and odd channels and a 3rd-order Gaussian-shaped OBPF with an optimized 20GHz bandwidth to demultiplex each channel.

All simulations were iterated with different random number seeds to give a total of around 200,000 simulated bits. The performance was evaluated in terms of the required normalized OSNR to achieve a bit error rate (BER) of 5×10^{-4} for the central channel by direct error counting, where

$$Normalized\ \ OSNR = \frac{Total\ Signal\ Power}{5\times Noise\ Power\ in\ 0.1nm} \qquad (12)$$

The pre-filtering in the proposed system was designed such that the spectral profile of the channel signal before demultiplexing, $H_s(\omega)$, was a 10GHz 8th-order Gaussian-shaped profile divided by $H_{D,j}(\omega+\omega_j)$. $H_s(\omega)$ contains contributions from the pre-filtering, DAC, driving amplifier, MZM electronic interface, CD etc, so pre-filtering would create a spectral profile equal to be the targeted $H_s(\omega)$ divided by the overall system response before demultiplexing.

Table 2 shows the calculated SCPR and SIPR for the conventional CoWDM and the pre-filtered multi-carrier system by using the method described in Section II. It can be clearly seen that the proposed technique can significantly improve the SCPR by 5.7dB and the SIPR by 2.6dB.

The effectiveness of the proposed pre-filtering technique is further depicted in Fig. 8, which shows the required normalized OSNR versus the phase difference between channels, ϕ, when the equivalent modulation bandwidth, including those of the driving amplifier and the modulator, is 6GHz (squares), 10GHz (circles), and 25GHz (triangles). In the figure, the performances of the pre-filtered system for the cases of 6GHz, 10GHz, and 25GHz were almost the same (<0.2dB), so only the curve for 10GHz was plotted. From the results, it can be clearly seen that, in conventional CoWDM, the performance depended on the phases of adjacent channels, and, as expected from the prediction in Fig. 6, the performance was optimized when ϕ was $\pi/2$, where the residual crosstalk field was approximately orthogonal to the signal field. Note that the "orthogonal" here is different from the channel "orthogonality" as described in this paper and should not be mixed in the concept. Fig. 9 shows the simulated constellation diagrams for conventional and pre-filtered systems at 20dB OSNR. These diagrams were obtained by disabling the laser linewidth and directly sampling the full optical field. The figures show that although controlling ϕ to be $\pi/2$ in conventional system improved the performance, it could not fundamentally reduce the crosstalk level, which was determined by the system response. In contrast, electronic pre-filtering reduced the crosstalk level (by 5.7dB as seen in Table 2). Consequently, the performance was greatly improved and the fluctuation in the required OSNR was less than 0.8dB, eliminating the need for the carrier phase control. In the following studies, unless otherwise stated, ϕ was set to be $\pi/2$.

Table 2. SCPR and SIPR for two different sets of spectral profiles

	SCPR	SIPR
Conventional system	10.3 dB	18.2dB
Pre-filtered system	16dB	20.8dB

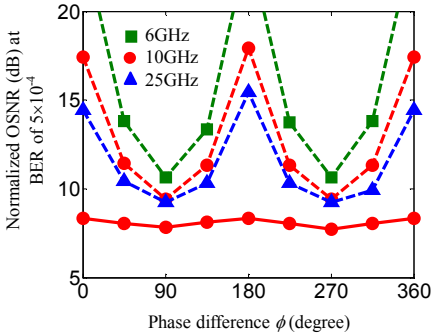


Fig. 8. Required normalized OSNR versus the phase difference between channels for conventional CoWDM (dashed) and the pre-filtered multi-carrier system (solid). Squares, circles, and triangles represent 6GHz, 10GHz, and 25GHz modulation bandwidth. The bandwidth of the DAC is fixed to be 8GHz.

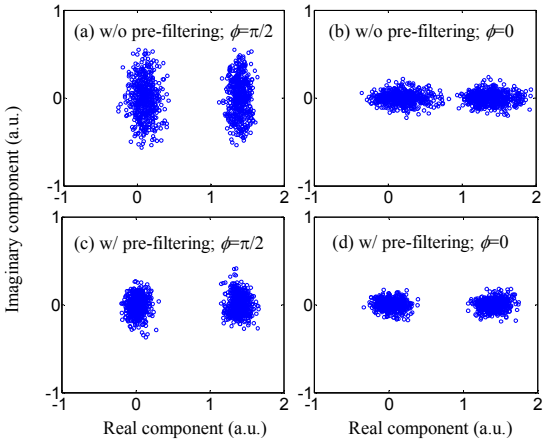


Fig. 9. Simulated constellation diagrams for conventional CoWDM ((a)-(b)) and the pre-filtered multi-carrier system ((c)-(d)) at 20dB OSNR when ϕ is $\pi/2$ ((a) and (c)) and 0 ((b) and (d)). The modulation bandwidth is 10GHz.

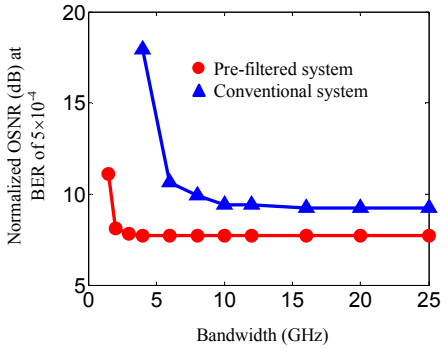


Fig. 10. Required normalized OSNR versus the equivalent bandwidth of the driving amplifier and the modulator.

Figure 10 illustrates the performance versus the equivalent modulation bandwidth. The DAC bandwidth was fixed to be 8GHz. Reducing the modulation bandwidth in conventional system severely increased the amount of ISI, and resulted in OSNR penalties even with the optimized phase. In contrast, the pre-filtering method, by pre-equalizing the modulation bandwidth and the remaining system response before channel demultiplexing, significantly relaxed the specifications and exhibited less than 0.5dB OSNR penalty for a modulation bandwidth as small as 2GHz.

In simulations, 8-bit physical DAC resolution was assumed. This value matched that of commercial arbitrary waveform generator. However, it would be desirable in practice to understand the performance penalties associated with the reduced DAC resolution. Fig. 11 shows the required OSNR as a function of the DAC resolution, from which it is seen that less than 0.5dB penalty was observed for 4-bit DAC resolution. This is readily achievable by commercial DAC products, which can have at least 6-bit physical resolution [23].

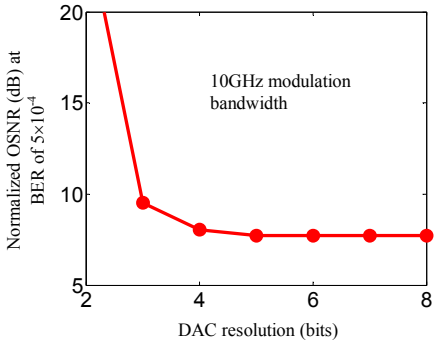


Fig. 11. Performance versus the DAC resolution in the pre-filtered system.

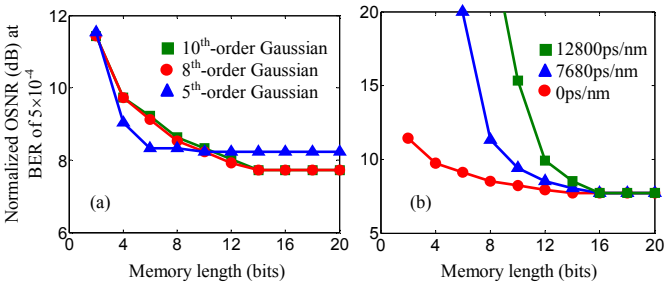


Fig. 12. Required OSNR versus the memory length of the transmitter-side FIR for (a) different targeted $H_s(\omega)$ spectral profiles; (b) different CD values.

The pre-filtering in the previous studies was designed to achieve a 10GHz 8th-order Gaussian-shaped signal profile divided by the transfer function of the demultiplxer ($H_{D,j}(\omega+\omega_j)$) at the input of the demultiplexing filter. Fig. 12(a) shows the performance versus the memory length of the transmitter-side FIR to obtain 5th- (triangles), 8th- (circles), and 10th-order (squares) Gaussian-shaped profiles divided by $H_{D,j}(\omega+\omega_j)$. A 5th-order Gaussian-shaped spectral profile required a smaller memory length to enable performance convergence, but exhibited the worst optimized performance. An 8th-order Gaussian profile was the best because, beyond this point, the performance was saturated and further increase of the Gaussian order could not mitigate the impairments evidently and only resulted in a larger penalty for small memory length values.

The pre-filtering takes into account the overall system response before channel demultiplexing, including CD. This aspect is similar to the well-known CD pre-distortion method [18]. Fig. 12(b) depicts the required OSNR versus the memory length for different CD values, and it was found that 16-bit memory length could fully compensate 12800ps/nm CD. Clearly, a larger memory length would allow for increased CD. In the following investigations (Section III and IV), the memory length of the transmitter-side FIR was set to be 16.

Figure 13(a) investigates the effect of fiber nonlinearity, and depicts the performance versus fiber length for the pre-filtered system when the signal launch power per channel is -1.5dBm (circles) and -6dBm (triangles). The pre-compensator is set to only compensate for the linear transmission impairments. The dashed line represents the case where the fiber nonlinear coefficient was set to be zero. The figure shows that approximately 2.5dB and 0.8dB OSNR penalties were observed for -1.5dBm and -6dBm signal power respectively. These penalties might be mitigated by incorporating an additional nonlinearity compensator into the transmitter-side DSP [24], although this would require more complex electronic circuits.

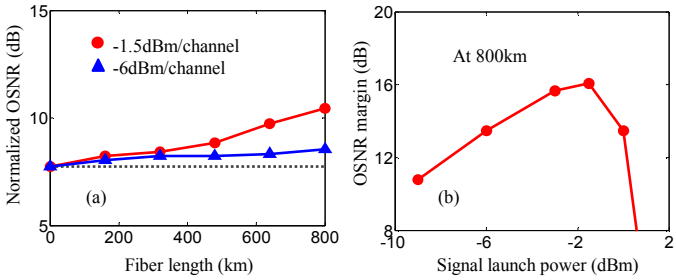


Fig. 13. (a) Performance versus fiber length for the pre-filtered system when the signal launch power per channel is -1.5dBm (circles) and -6dBm (triangle). Dashed line represents the case without the fiber nonlinearity. (b) OSNR margin versus the signal launch power per channel for the pre-filtered system.

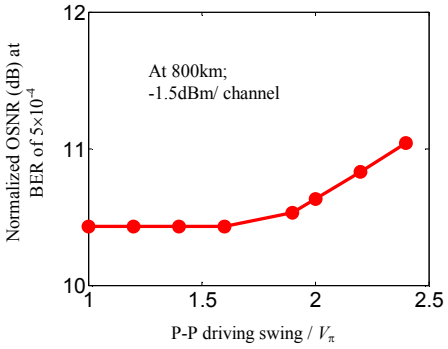


Fig. 14. Required OSNR versus the driving voltage of the pre-filtered signal into the modulators at 800km.

The optimal signal launch power was related to not only the OSNR penalty induced by the fiber nonlinearity but also the maximum received OSNR. The OSNR margin versus the launch power is depicted in Fig. 13(b). The figure shows that when the signal launch power was less than -1.5dBm, the OSNR margin was improved because the received OSNR increased with the input power. However, when the launch power was larger than -1.5dBm, the penalty induced by the fiber nonlinearity increased significantly whilst the maximum received OSNR still increased linearly proportional to the signal launch power, resulting in a reduced OSNR margin.

We also investigated the nonlinear effects due to the signal modulation with MZMs. Fig. 14 depicts the required OSNR versus the peak-to-peak driving swing of the pre-filtered signal into the MZMs at 800km. The MZMs exhibited a cosine-shaped transfer function, and a large pre-filtered signal level into the MZM resulted in nonlinear distortion. The figure shows that the penalty induced by this effect was negligible for $1.6V_\pi$ and was less than 0.3dB when using a full driving voltage ($2V_\pi$).

IV. Combination of Pre-shaping and Post-filtering

Section III has clearly shown the benefit of the pre-filtering technique to improve the system performance and relax the specifications of transmitter-side devices. In this section, we will further combine the pre-shaping technique with receiver-side post-filtering, and numerically demonstrate its use in QPSK-based multi-carrier system with channel spacing equal to the symbol rate per carrier. The performance comparison shows that this method outperforms conventional QPSK-based system without DSP [2-3] or with only receiver-side DSP [4], especially when the responses of the transmitter and the demultiplexing filter are not precisely designed and the sampling rate of the analogue-to-digital converter (ADC) is not sufficiently high, resulting in severe residual crosstalk and ISI.

Figure 15 shows the simulation setup. The transmitter and the fiber link were similar to those used in Fig. 7, and so are only described briefly here. Uncorrelated 10Gsym/s QPSK data trains were pre-filtered by 2samples/sym FIR filter with 16-bit memory length. The DACs had 8-bit physical resolution and each digital sample generated a 20-sample rectangular pulse to emulate the analogue signals. The frequency response of the DAC was 8GHz 2rd-order Gaussian-shaped, whilst that for the driving amplifier and the modulator was 10GHz 5th-order Bessel-shaped. The peak-to-peak driving swing of the electrical signal into the modulator was $1.6V_\pi$. The laser had 100kHz linewidth, and the phases of the carriers were controlled to be 0, ϕ, 2ϕ, 3ϕ, 4ϕ. It should be noted that these phase controls were only used to investigate the performance as a function of carrier phases, and as will be shown in Fig. 17, are not required in either the proposed system or conventional QPSK-based system such as no-guard-interval optical coherent OFDM [3-4]. Therefore, these systems are not "CoWDM". The fiber link consisted of spans of 80km SMF with varied signal launch power. The step length of the split step Fourier method for signal propagation in the fiber was selected for each signal power to ensure calculation accuracy. The optical amplifiers had 4dB NF.

At the receiver, the signal power into the preamplifier was adjusted to control the OSNR. The bandwidth of the OBPF was varied to illustrate the robustness of the proposed method to the filter bandwidth. Coherent detection was used. The signal and local oscillator were mixed by a 90^0 optical hybrid, and detected by balanced detectors to extract the in-phase and quadrature components. The powers of the local oscillator and the received signal were 10dBm and -3dBm, and their polarizations were controlled to be the same. The equivalent thermal noise spectral power density of the detectors was $20pA/Hz^{1/2}$. After detection, the signals were electrically amplified and filtered by 4th-order Bessel EFs. The bandwidth of the EFs was found to play an important role in system performance, and was varied for investigation. The received analogue signals were sampled by ADCs with two or four samples per symbol. The sampled signals were fed into a FIR filter, which employed mean-square error criterion to update the FIR coefficients every symbol [17]. The equalized signal was further down-sampled to one sample per symbol, before it was phase estimated and decoded [25].

For comparison, conventional QPSK-based system without DSP [3] or with only receiver-side DSP [4] was also simulated. A high-level setup for multiplexing and demultiplexing was shown in Fig. 3 while the transmission link was the same as that in Fig. 15. The electrical data trains were raised-cosine shaped with a roll-off coefficient of 0.4. These signals were fed directly into the driving amplifiers by bypassing the FIR filter and DACs as used in Fig. 15. The equivalent frequency response of the driving amplifier and the modulator's electronic interface was also 5th-order Bessel shaped with 10GHz bandwidth. The optical demultiplexing filter comprised an AMZI with 20GHz FSR and a 3rd-order Gaussian-shaped OBPF with an optimized bandwidth of 25GHz, unless otherwise stated. The parameters of coherent detector and electrical filters were the same as those in Fig. 15. For conventional QPSK system without DSP, the received signal was sampled with one sample per symbol, phase estimated and decoded. On the other hand, the system using only receiver-side DSP employed 2 or 4samples/sym ADCs, and an additional FIR filter was used to adaptively balance the

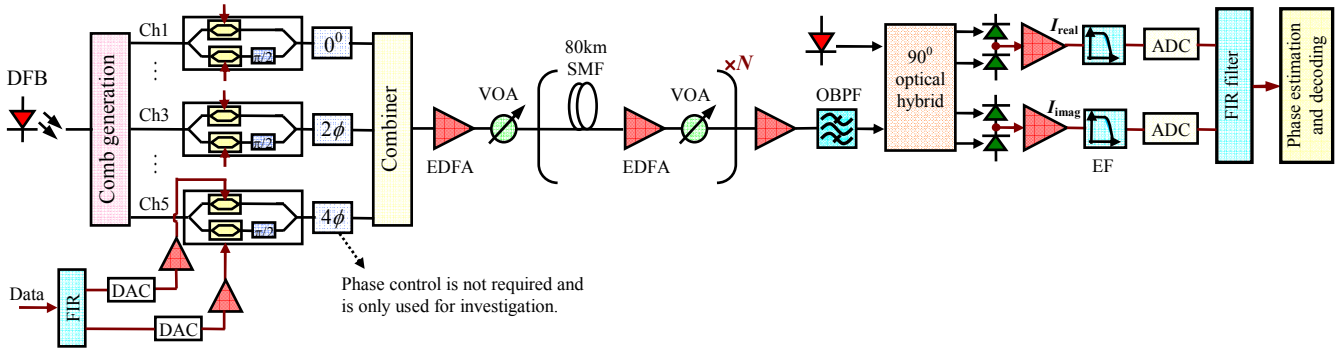


Fig. 15: Simulation setup of a coherent-detection QPSK-based multi-carrier system with channel spacing equal to the symbol rate per carrier using a combination of pre-shaping and post-filtering.

crosstalk and ISI before phase estimation and decoding.

It should be noted that in principle, OBPF is not necessarily used in coherent detection in Fig. 15 because in a linear receiver, any functionality of an OBPF can be performed by a digital filter provided that the sampling rate of ADC is sufficiently high to avoid aliasing. However, in this paper, we used an OBPF for comparison with recently published systems [2-4] and to illustrate the relaxed requirement of the ADC sampling rate for the proposed system (see Fig. 18).

Figure 16 shows the performance versus the memory length of receiver-side FIR at 2samples/sym when the transmitter FIR and the optical demultiplexing filter are the same as those used in Section III. The dotted line represents the theoretical limit for a single-channel 10Gsym/s QPSK signal [26]. The point of zero memory length corresponds to the case using only the transmitter-side FIR, and it can be seen that combined DSP, by adaptively trimming the demultiplexing filter as well, further improved the back-to-back sensitivity by 1dB for memory lengths larger than 10 bits. This performance improvement results in the penalty reduction to only 1dB beyond the theoretical limit. In the following study, the memory length of the receiver-side FIR was 10 bits.

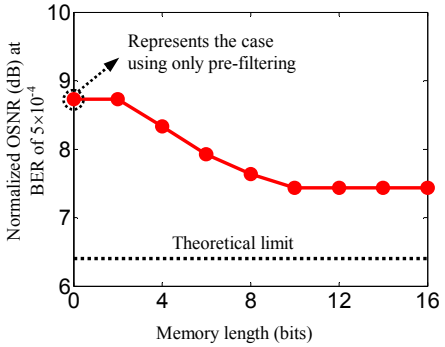


Fig. 16. Required OSNR versus the memory length of the receiver-side FIR filter when the transmitter-side FIR filter and the optical demultiplexing filter are the same as those used in Section III. Receiver EF is 15GHz. The dotted line represents the theoretical limit for a single-channel 10Gsym/s QPSK signal.

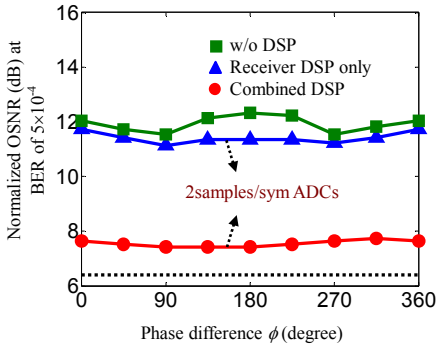


Fig. 17. Performance versus ϕ when the receiver-side FIR is 2samples/sym and the modulation bandwidth is 10GHz. Receiver EF is 15GHz.

The proposed technique also significantly outperformed the conventional system without DSP or with only receiver-side DSP, as shown in Fig. 17, which illustrates the required OSNR versus the phase difference between channels. In the figure, the bandwidth of the OBPF was optimized for each case and that of the EF was fixed at 15GHz. The conventional system with only receiver-side FIR and the proposed method with combined DSP both employed 2samples/sym ADCs. The dotted line represents the theoretical limit for a single-channel 10Gsym/s QPSK signal. As expected (Fig. 6), the performance of conventional QPSK-based system without DSP (squares) was nearly independent of the phase, with only around 0.6dB OSNR fluctuation. The system using only receiver-side DSP (triangles) did not exhibit much performance benefits at 2samples/sym. In contrast, combined DSP (circles), by precisely shaping the signal spectrum as well as the demultiplexing filter to bandwidth limited near-rectangular profile, significantly improved the performance, and over 4dB receiver sensitivity improvement was obtained even at 2samples/sym. Note that the combined DSP still does not achieve ideal ISI and crosstalk free operation, with 1dB penalty beyond the theoretical limit. The increased sensitivity of higher-order quadrature amplitude modulation (QAM) to non-ideal system response would further enhance the penalty. Using the combined DSP configuration, this penalty would increase to more than 6dB for 16QAM, suggesting the necessity of either enhanced DSP or alternative strategies to achieve satisfactory performance.

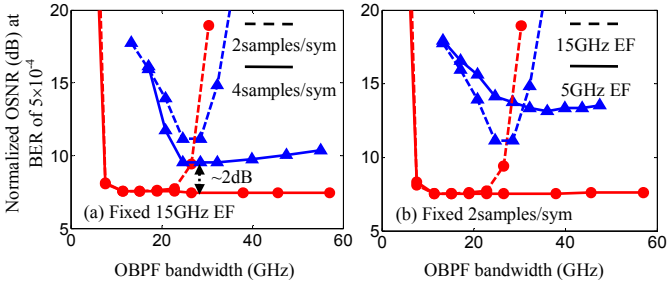


Fig. 18. Required OSNR versus the OBPF bandwidth for (a) a fixed EF bandwidth and varied ADC sampling rate, (b) fixed 2samples/sym ADCs and varied EF bandwidth. Circles and triangles represent the cases using combined DSP and only receiver-side DSP respectively.

In Fig. 17, the sampling rate of the ADCs was 2samples/sym and the receiver EF had a 15GHz bandwidth. These two parameters were closely related to the system performance and the required specification of the OBPF. Fig. 18(a) depicts the required OSNR versus the OBPF bandwidth for combined DSP (circles) and only receiver-side DSP (triangles) with different ADC sampling rate and 15GHz EF. The figure shows that when using 2samples/sym (dashed), the performance of both scenarios was severely degraded for the OBPF bandwidth larger than 30GHz due to aliasing in the ADCs. The combined DSP exhibited a wider bandwidth tolerance range and a better performance than using only receiver-side DSP. By increasing the ADC sampling rate to avoid aliasing (solid), the tolerance ranges of the OBPF bandwidth for both scenarios were improved. The performance of the conventional system became steady for the OBPF bandwidth larger than 25GHz, and the optimal receiver sensitivity was improved by around 1.5dB. This performance improvement matched the experimental observations [4]. On the other hand, combined DSP showed optimal performance as long as the bandwidth was larger than 7GHz, with 2dB better OSNR sensitivity than that using only

receiver-side DSP.

A higher ADC sampling rate inevitably increases the implementation complexity. The proposed method can relax this requirement by employing an EF with a smaller bandwidth to avoid the aliasing effect. Fig. 18(b) shows the required OSNR versus the OBPF bandwidth for 15GHz (dashed) and 5GHz (solid) EF at 2samples/sym. It can be seen that by using 5GHz EF bandwidth, the system using combined DSP could also extend the tolerance range of the OBPF bandwidth beyond 30GHz even for 2samples/sym. In contrast, without trimming the signal pulse shape at the transmitter, the reduction of the EF bandwidth resulted in more distortions, and degraded the optimal performance. Fig. 18(a) and (b) suggest the capability of the combined DSP to improve the system performance and to relax the specifications of the OBPF and the ADCs.

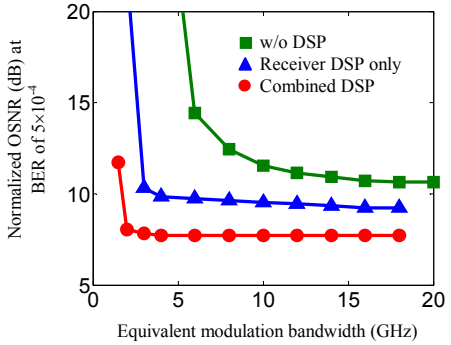


Fig. 19. Required OSNR versus the modulation bandwidth. The ADC sampling rate for the system using only receiver-side DSP is 4samples/sym whilst that for the proposed system using combined DSP is 2samples/sym.

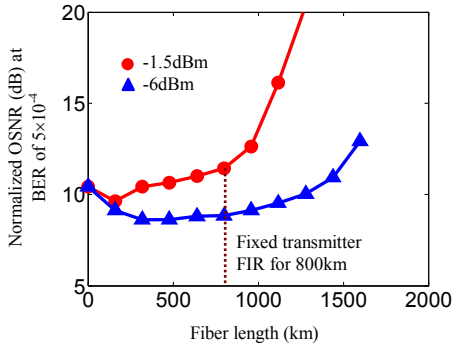


Fig. 20. Performance versus the fiber length for a system with a fixed transmitter-side FIR to fully compensate 800km CD and an adaptive receiver-side FIR to compensate the residual CD.

In addition to the relaxed specifications of the receiver-side components, the combined DSP also had improved tolerance to the modulation bandwidth, as illustrated in Fig. 19. In the figure, the system using combined DSP with 2samples/sym and 5GHz EF (circles) is compared to the system using only receiver-side DSP with 4samples/sym ADCs and 15GHz EF (triangles) and the conventional system without DSP (squares). The figure shows that the system using only receiver-side DSP at 4samples/sym improved the tolerance range of the modulation bandwidth when compared to the conventional system without DSP. The combined DSP further enhanced the tolerance and supported the transmitter-side bandwidth reduction to 2GHz. Note that in these multi-carrier systems with severely limited modulation bandwidth, the effect of ISI dominated and the functionality of re-shaping was, to a certain extent, similar to that in conventional WDM [19].

The combination of the pre-filtering and post processing also enhanced the system capability for adaptive CD compensation. Although it was shown in Section III that the transmitter-side filtering effectively compensated the CD, prior information on the CD value in the fiber link should be known. This information is usually obtained at the receiver, so the adaptation speed is limited due to the round-trip delay. By combining the pre-filtering with fixed FIR coefficients for preliminary CD compensation and the receiver-side DSP to adaptively mitigate the residual impairment, the system capability for adaptive CD compensation could be greatly improved. Fig. 20 shows the performance versus the fiber length when the transmitter-side FIR coefficients are fixed to fully compensate 800km CD, while those of the receiver-side FIR (10-bit memory length) adaptively trim the residual CD. Circles and triangles represent the cases when the signal launch power per channel is -1.5dBm and -6dBm respectively. The curve for a lower signal launch power was more symmetric at the point of 800km due to the smaller fiber nonlinearities. The figure clearly shows that when a -6dBm launch power was used, the system could support 1500km transmission with adaptive CD compensation. Clearly, this range could be increased by using longer memory lengths in the transmitter- and receiver-side FIRs.

V. Conclusions

We have systematically investigated an electronic signal processing technique to significantly improve the performance and relax the device specifications in optically multiplexed multi-carrier systems with channel spacing equal to the symbol rate per carrier. We have provided a generalized framework and theoretically shown that achieving perfect orthogonality between channels in these systems, together with ISI free operation as needed in generic communication systems, requires the shaping of the spectral profiles of not only the demultiplexing filter, but also the signal of each channel before demultiplexing. A novel semi-analytical method is proposed to quantitatively analyze the residual crosstalk and ISI levels arising from non-ideal system response in practical systems. Based on the implications of the analysis, we show that DSP, by precisely shaping these two spectral profiles, overcomes the limitations in the fabrication of high-speed analogue devices. We have studied the pre-filtering technique in direct-detection OOK-based system to ensure that the system response before channel demultiplexing approaches the targeted condition. It is shown that this method can greatly mitigate the inter-channel crosstalk level such that the technique of CoWDM, with additional phase control to mitigate the impact of the crosstalk in single-quadrature formats, is not required. We have further combined pre-shaping and post-filtering, and demonstrated its use in coherent detection QPSK-based system. It is shown that this technique outperforms conventional QPSK-based system without DSP or with only receiver-side DSP, with only 1dB penalty beyond the theoretical limit even for a receiver sampling

rate as low as 2samples/sym. In addition, the inclusion of ISI free operation, with this aspect similar to that in conventional WDM, allows the relaxation of the modulation bandwidth and CD compensation.

REFERENCES

[1]. H. Sanjoh, E. Yamada, and Y. Yoshikuni, "Optical orthogonal frequency division multiplexing using frequency/time domain filtering for high spectral efficiency up to 1bit/s/Hz", *Optical Fiber Communication Conference*, ThD1, 2002.

[2]. A. Sano, H. Masuda, E. Yoshida, T. Kobayashi, E. Yamada, Y. Miyamoto, F. Inuzuka, Y. Hibino, Y. Takatori, K. Hagimoto, T. Yamada, and Y. Sakamaki, "30x100 Gb/s all-optical OFDM transmission over 1300 km SMF with 10 ROADM nodes", *European Conference on Optical Communication*, PD1.7, 2007.

[3]. A. Sano, E. Yamada, H. Masuda, E. Yamazaki, T. Kobayashi, E. Yoshida, Y. Miyamoto, R. Kudo, K. Ishihara, and Y. Takatori, "No-guard-interval coherent optical OFDM for 100Gb/s long-haul WDM transmission," *IEEE J. Lightwave Technol.*, vol. 27, 3705-3713, 2009.

[4]. S. Chandrasekhar, X. Liu, "Experimental investigation on the performance of closely spaced multi-carrier PDM-QPSK with digital coherent detection," *Opt. Express*, vol. 17, pp. 21350-21361, 2009.

[5]. X. Liu, S. Chandrasekhar, B. Zhu, and D.W. Peckham, "Efficient digital coherent detection of a 1.2Tb/s 24-carrier no-guard-interval Co-OFDM signal by simultaneously detecting multiple carriers per sampling," *Optical Fiber Communication Conference*, OWO2, 2010.

[6]. G. Goldfarb, G. Li, and M.G. Taylor, "Orthogonal wavelength division multiplexing using coherent detection," *IEEE Photon. Technol. Lett.*, vol. 19, 2015-2017, 2007.

[7]. A.D. Ellis, F.C.G. Gunning, "Spectral density enhancement using coherent WDM," *IEEE Photon. Technol. Lett.*, vol. 17, 504-506, 2005.

[8]. F.C.G. Gunning, T. Healy, A.D. Ellis, "Dispersion tolerance of coherent WDM," *IEEE Photon. Technol. Lett.*, vol. 18, 1338-1340, 2006.

[9]. S. Ibrahim, A.D. Ellis, F.C.G. Gunning, F.H. Peters, "Demonstration of CoWDM using DPSK modulator array with injection-locked lasers," *Electronics Letters*, vol. 46, 150-152, 2010.

[10]. W. Shieh, H. Bao, and Y. Tang, "Coherent optical OFDM: theory and design," *Opt. Express*, vol. 16, pp. 841-859, 2008.

[11]. S.L. Jansen, A.A. Amin, H. Takahashi, I. Morita, and H. Tanaka, "132.2-Gb/s PDM-8QAM-OFDM transmission at 4-b/s/Hz spectral efficiency," *IEEE Photon. Technol. Lett.*, vol. 21, pp. 802-804, 2009.

[12]. A.J. Lowery, L.B. Du, and J. Armstrong, "Performance of optical OFDM in ultra long-haul WDM lightwave systems," *IEEE J. Lightwave Technol.*, vol. 25, pp. 131-138, 2007.

[13]. R.W. Chang, "Synthesis of band-limited orthogonal signals for multi-channel data transmission," *Bell Syst. Tech. J.*, vol. 45, pp. 1775-1796, 1966.

[14]. S.B. Weinstein and P. M Ebert, "Data transmission by frequency division multiplexing using the discrete Fourier transform," *IEEE Trans. Commun. Technol.*, vol. COM-19, pp.628-634, 1971.

[15]. K. Takiguchi, M. Oguma, T. Shibata, and H. Takahashi, "Optical OFDM demultiplexer using silica PLC based optical FFT circuit," *Optical Fiber Communication Conference*, OWO3, 2009.

[16]. D.O. North, "An analysis of the factors which determine signal/noise discrimination in pulse carrier systems," *RCA Tech. Report*, no. 6 PTR-6C, 1943.

[17]. J. Proakis, *Digital Communication*, 4th Edition, McGraw-Hill, 2001.

[18]. M. O'Sullivan, K. Roberts, and C. Bontu, "Electronic dispersion compensation techniques for optical communication systems", *European Conference on Optical Communication* (2005), paper Tu3.2.1.

[19]. X. Zhou, J. Yu, M.F. Huang, Y. Shao, T. Wang, L. Nelson, P. Magill, M. Birk, P.I. Borel, D.W. Peckham, and R.Lingle, "64Tb/s (640×107Gb/s) PDM-36QAM transmission over 320km using both pre- and post-transmission digital equalization," *Optical Fiber Communication Conference*, PDPB9, 2010.

[20]. G. Gavioli, E. Torrengo, G. Bosco, A. Carena, V. Curri, V. Miot, P. Poggiolini, M. Belmonte, F. Forghieri, C. Muzio, S. Piciaccia, A. Brinciotti, A.L. Porta, C. Lezzi, S. Savory, S. Abrate, "Investigation of the impact of ultra-narrow carrier spacing on the transmission of a 10-carrier 1Tb/s superchannel," *Optical Fiber Communication Conference*, OThD3, 2010.

[21]. J. Zhao and A. D. Ellis, "Electronic signal processing for crosstalk- and ISI-free operation in all-optical OFDM," *European Conference on Optical Communication*, Tu.4.A.7, 2010.

[22]. P.J. Winzer, M. Pfennigbauer, and R.J. Essiambre, "Coherent crosstalk in ultradense WDM systems," *IEEE J. Lightwave Technol.*, vol. 23, pp. 1734-1744, 2010.

[23]. T. Ellermeyer, J. Mullrich, J. Rupeter, H. Langenhagen, A. Bielik, and M. Moller, "DA and AD converters for 25 GS/s and above," *IEEE/LEOS Summer Topical Meetings,* pp. 117-118, 2008.

[24]. R.I. Killey, P.M. Watts, P. Bayvel, ''Electronic pre-compensation techniques to combat dispersion and nonlinearities in optical transmission," *European Conference on Optical Communication* (2005), paper Tu4.2.1.

[25]. Ivan P. Kaminow, T. Li, A.E. Willner, *Optical Fiber Telecommunications V B*, 5th Edition, Elsevier, 2008.

[26]. A.D. Ellis, J. Zhao, D. Cotter, "Approaching the non-linear Shaonnon limit," *IEEE J. Lightwave Technol.*, vol. 28, pp. 423-433, 2010.

Jian Zhao received the B.Eng. degree from University of Science and Technology of China (USTC) in 2002, and the M.Phil. and Ph.D. degrees from the Chinese University of Hong Kong (CUHK) in 2004 and 2007, respectively.

During 2002–2004, he worked on supercontinuum-based photonic devices for multi-wavelength optical networks. In his Ph.D. program (2004–2007), his research interests included electronic signal processing and advanced modulation formats in optical communication and wavelength-division multiplexing passive optical networks. He joined the Photonic Systems Group at the Tyndall National Institute as a Postdoctoral Research Scientist in August 2007. His current research interests include electronic signal processing in optical communications and spectrally-efficient multi-carrier optical transmission systems. He has published 50 technical papers in peer-reviewed international journals and conferences and 2 patents.

Dr. Zhao is an Enterprise Ireland principal investigator and was the recipient of the First Prize of Outstanding Student Scholarship of USTC. He acts as a reviewer for IEEE Photonics Technology Letters, Optics Express, and Optics Communications etc.

Andrew Ellis received the B.Sc. degree in physics with a minor in mathematics from the University of Sussex, Brighton, U.K., in 1987. He received the Ph.D. degree in electronic and electrical engineering from The University of Aston in Birmingham, Birmingham, U.K., in 1997 for his study on all optical networking beyond 10 Gbit/s.

He previously worked for British Telecom Research Laboratories as a Senior Research Engineer investigating the use of optical amplifiers and advanced modulation formats in optical networks and the Corning Research Centre as a Senior Research Fellow where he led activities in optical component characterisation. Currently, he heads the Transmission and Sensors Group at the Tyndall National Institute in Cork, Ireland, where he is also a member of the Department of Physics, University College Cork. He research interests include the evolution of core and metro networks, and the application of photonics to sensing. He has published over 100 journal papers and over 20 patents in the field of photonics.

Dr. Ellis is a member of the Institute of Physics and the Institute of Engineering Technology, and is a Chartered Physicist. He acts as a reviewer for IEEE Journal of Lightwave Technology, IEEE Photonics Technology Letters etc, and as an associated editor for Optics Express. He has served as member of the Technical Program Committees for many international conferences, including OFC/NFOEC and ECOC etc.